DOI: 10.1002/ejic.201100756

Structural Relationship between Calcite–Gelatine Composites and Biogenic (Human) Otoconia

Paul Simon,[a] Wilder Carrillo-Cabrera,[a] Ya-Xi Huang,[b] Jana Buder,[a] Horst Borrmann,[a] Raul Cardoso-Gil,[a] Elena Rosseeva,[a] Yuri Yarin,[c] Thomas Zahnert,[c] and Rüdiger Kniep*[a]

Keywords: Biomimetic synthesis / Biomineralization / Organic-inorganic composites / Structure determination / Human otoconia / Calcite

Biogenic otoconia (ear dust) are composite materials of calcite with about 2 wt.-% proteins showing an average longitudinal size of about 10 μm. The tiny biomineral particles are situated in the inner ear (in the maculae) and act as sensors for gravity and linear acceleration. Our comparative study of calcite–gelatine composites (grown by double diffusion) and human otoconia is based on decalcification experiments, scanning electron microscopy, TEM and X-ray investigations in order to obtain a complete picture of the 3D structure and morphogenesis of the materials. Otoconia as calcite–protein composites display a cylindrical body with terminal rhombohedral faces intersecting at the pointed ends. As evidenced by TEM on focused ion beam cuts, both the artificial composites and human otoconia show a particular distribution of areas with different volume densities leading to a dumbbell-shape of the more dense parts consisting of rhombohedral branches (with end faces) and a less ordered, less dense area (the belly region). The peculiar inner architecture of otoconia with its dumbbell-shaped mass/density distribution is assumed to be necessary for optimal sensing of linear accelerations.

Introduction

The inner ear of vertebrates contains a complex arrangement of enclosed sacs and channels where the senses of balance and hearing are located.[1] Parts of these sensory systems are called maculae. These organs act as gravity receptors by responding to linear accelerations.[2] The sensory transduction depends on the inertial mass of a calcium carbonate biomineral (statolith). In the case of fish and amphibians, this consists of aragonite or sometimes vaterite (otoliths),[3,4] whereas calcite modification (otoconia) is found in reptiles, birds and mammals.[2] A major difference between otoliths (ear stones; mm sized)[5] and otoconia (ear dust; μm sized)[6] is that otoliths display a daily growth pattern, whereas adult otoconia are essentially inert and undergo only small changes with time. Furthermore, the otoconia are made up of thousands of tiny biomineral particles, each showing a barrel-shaped habit with triplanar faceted ends.[6–8] Scanning electron microscopy (SEM) images of human otoconia with the typical barrel shaped morphology are presented in Figure 1 (a and b). The peculiar shape of otoconia as well as their inner structure and resulting biofunctionality are little understood. The same is true of the shape development (morphogenesis).

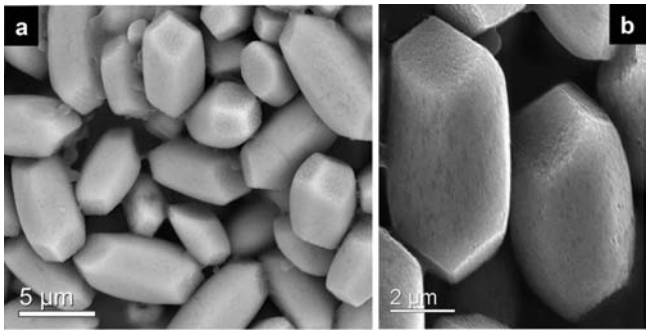

Figure 1. SEM images of human otoconia. (a) Overview of several specimens and (b) image of individuals showing their barrel-shaped morphology and faceted ends.

This report contributes to these questions by a comparative study (artificial/biogenic) and describes the development of a complex composite architecture. The calcite–gelatine composites were grown by double diffusion in gelatine-gel matrices.[9] Human otoconia were isolated by one of the authors (Yu. Y.).

[a] Anorganische Chemie, Max-Planck-Institut für Chemische Physik fester Stoffe,
Nöthnitzer Str. 40, 01187 Dresden, Germany
Fax: +49-351-4646 3002
E-mail: Kniep@cpfs.mpg.de
[b] College of Materials, Xiamen University,
Kexue Building 316, Xiamen 361005, Fujian Province, China
[c] Klinik und Poliklinik für HNO-Heilkunde, Universitätsklinik Carl Gustav Carus, TU Dresden,
Fetscherstr. 74, 01307 Dresden, Germany

Characteristic Features of Human Otoconia

The following features (data taken from literature) seem to be evident for otoconia of mammals, although the various aspects reported do not form a conclusive picture:

(i) The typical (adult) configuration of either saccular or utricular otoconia is a cylindrical body with terminal rhombohedral faces intersecting at the pointed ends. The symmetry of otoconia is close to $-3m$ (depending on the size of the rhombohedral faces, which may be different).[8,10,11]

(ii) Otoconia represent composite systems that comprise ordered calcite microcrystals together with organic molecules (mainly glycoproteins and glycosaminoglycans), which form fibril arrangements within the composite.[8,12,13]

(iii) No reliable data concerning the amount of organic components in the internal otoconial matrix are available to date. It has been estimated that the content of organic material for the rat otoconial complex (otoconia + otoconial membrane) is less than 10 wt.-%.[14] However, these data do not represent the amount of organic material directly within the otoconia. Therefore, a value of about 2.25 wt.-%, which has been reported for aragonitic plaice otoliths,[10] may be used as an approximate guideline. This value is representative for biocomposites that contain small amounts of organic material and is generally consistent with a report on mammalian otoconia that were described as containing only "small" amounts of organic material (proteins).[8,14,15]

(iv) At least two different structures are present in otoconia: A first, more dense structure and a second, more porous one.[8] The higher material density seems to be present towards the rhombohedral end faces.[11]

(v) The mean size (length) of otoconia is about 10 μm[16] and giant otoconia of up to 80 μm in length have been observed.[17]

(vi) There are some indications that (at least parts of) otoconial specimens behave as single crystals.[10,18,19]

Although so far unconfirmed, it can be expected that otoconia, which are grown during biomineralisation processes, represent nanoscale inorganic–organic composites. If these otoconia give rise to Bragg scattering properties similar to those of single crystals (see feature vi) they may represent highly mosaic-controlled nanocomposite superstructures in a similar sense as reported for biomimetic apatite–gelatine nanocomposites.[20–24] This kind of solid matter is also called a mesocrystalline state.[25]

Results and Discussion

Morphology and Morphogenesis of Calcite–Gelatine Composite Individuals and Biogenic Otoconia

The calcite–gelatine composites contain an amount of gelatine between 1.9 and 2.6 wt.-%,[9] which is in good agreement with 2.25 wt.-% observed for aragonitic plaice otoliths.[10] The composite nature of the artificial specimen is associated with a lower density (2.563 $g cm^{-3}$)[9] than a bulk calcite crystal (2.711 $g cm^{-3}$). Furthermore, the density of the artificial specimen is similar to the values determined for rat otoconia (2.47–2.65 $g cm^{-3}$).[26] The planar terminal faces of the artificial individuals are indexed as normal rhombohedral faces (cleavage rhombohedra of calcite).[9]

In addition to the more pronounced, rounded belly region, in their final state of development the artificial composites reveal analogous morphological characteristics to those observed for adult otoconia of mammals and humans (Figures 1 and 2) with an overall symmetry close to $-3m$. Comparison to biogenic otoconia, the artificial composite specimens have to be classified as "more than giant".[17] Artificial samples investigated after a growth period of five days consist of composite particles in their final state of shape development with a size distribution between 100 and 400 μm. Our observations also indicate that the shape development to the closed otoconial habit may be complete at a size of around 100 μm.

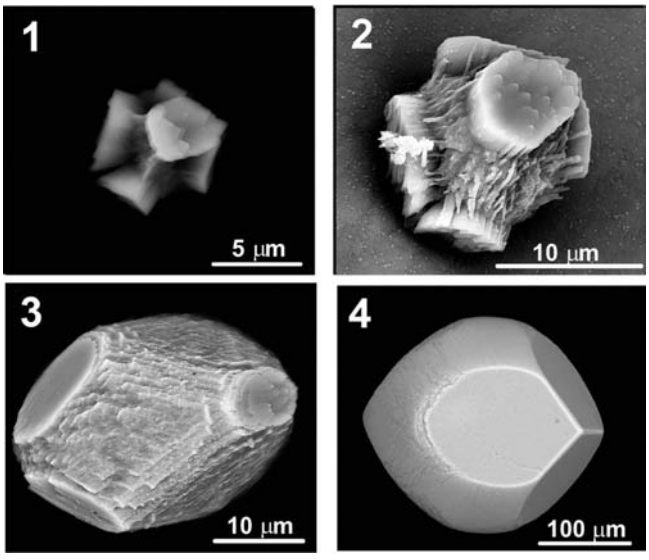

Figure 2. Morphogenesis of calcite–gelatine composite individuals grown by double diffusion in gelatine-gel matrices. Growth sequence 1–4 taken from ref.[9b] For further details see text.

The formation of calcite–gelatine composites was first observed during our work on the morphogenesis of carbonated apatite–gelatine nanocomposites by double diffusion in gelatine-gel matrices.[9,27] The otoconia-shaped specimens grow close to the calcium ion source and their complex morphogenesis is shown in Figure 2. Within days, the shape development evolves from stage 1 (an arrangement characterised by six trumpet-like branches) via various intermediate states that are dominated by six branches (stages 2–3). The branches grow fast and develop their basal faces to the final state (stage 4) where they meet at both ends, thereby each forming three planar faces with straight common edges and rounded boundaries in the direction of the belly region. The belly region grows with temporal delay and appears to be structured on a small particle scale but with a preferred (common) orientation of the subunits. Similar observations have been made by Dickman et al.[28] on the embryonic states of otoconia extracted from the utricular macula of Japanese quail (Figure 3, a). In analogy to the

artificial composite individuals, in six days of embryonic growth, six trumpet-like branches are present with trihedral faceted ends. Utricular otoconia at the mature stage of development in the central macula of adult animals are shown in Figure 3 (b).[28]

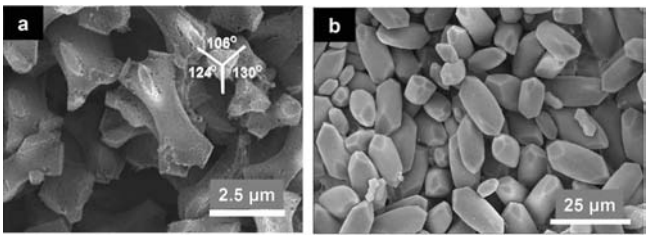

Figure 3. (a) SEM micrographs of the embryonic states (sixth day) of otoconia extracted from the utricular macula of Japanese quail, which display six branches with faceted ends. (b) Barrel-shaped mature states of utricular otoconia of Japanese quail.[28]

Crystallographic Characterisation of Artificial (Otoconia-Shaped) Individuals and Human Otoconia

We investigated the X-ray diffraction behaviour (Ag-K_α radiation) of a complete single human otoconial specimen (ca. 10 µm in length). For this purpose, the sample was glued to a thin glass capillary (Figure 4, b). As can be seen from Figure 4 (d), the Bragg part of the diffraction pattern is representative of a single crystal (in the sense of a mesocrystal).[25] The crystal structure (calcite) of the human otoconia was solved from the diffraction data [$R\bar{3}c$, Z_H = 6, a_H = 4.9836(7) Å, c_H = 17.071(4) Å, $R1$ = 0.068; see Exp. Sect.]. In this respect, biogenic and artificial otoconia (Figure 4, a and b) show identical diffraction characteristics (Figure 4, c and d). By using a complete single artificial specimen, the crystal structure (calcite) was also solved [$R\bar{3}c$, Z_H = 6, a_H = 4.9880(4) Å c_H = 17.096(2) Å, $R1$ = 0.025; see Exp. Sect.].[9] The calcite subindividuals within the artificial and biogenic specimens were arranged in a way that an overall 3D periodic arrangement of the atoms forming the inorganic part of the composites was realised. The 3D periodic arrangement of atoms, however, is sharply affected by defects and disorder (mosaic structure), which is common for biominerals representing the mesocrystalline state.[25] The organic components of the composites do not significantly contribute to the Bragg parts of the diffraction images, although they are arranged to form specific patterns on the nano- and mesoscale. This situation will be shown and discussed in the following sections.

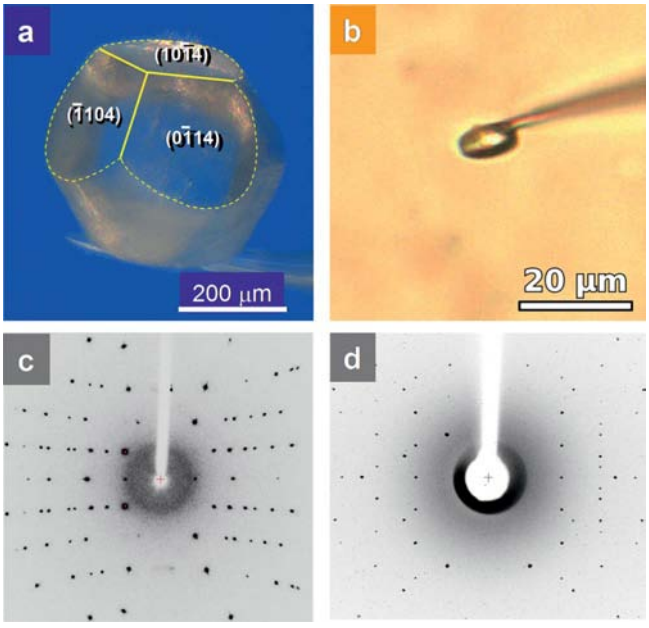

Figure 4. (a) Completely developed specimen of the calcite–gelatine composite glued to a glass capillary for X-ray investigations (optical microscopy image). The planar faces at both ends were determined to be normal rhombohedral faces (cleavage rhombohedra of calcite, taken from ref.[9b]). (b) Optical micrograph of a single human otoconial specimen glued to a glass capillary and used for the diffraction experiment. (c) The biomimetic individual shown in (a) exhibits Bragg diffraction properties representative of a single crystal (Mo-K_α radiation). The crystal structure (calcite) was solved from the diffraction data (taken from ref.[9b]). (d) X-ray diffraction pattern (Ag-K_α radiation) of the human otoconial specimen shown in (b). The crystal structure (calcite) was solved from the diffraction data.

Before coming to more detailed descriptions, some of the main features of the artificial and biogenic individuals are summarised in Table 1, which shows the close relationships of the individuals up to this point in the investigation.

Table 1. Comparison of some essential features of human otoconia and calcite–gelatine composite individuals. The good agreement between these overall characteristics led to more detailed investigations (vide infra).

	Artificial	Biogenic (Human)
$CaCO_3$/modification	calcite	
Amount organic	1.9–2.5 wt.-%[9]	max. 3.2 wt.-% (incl. surface organics)[a]
Overall shape	–3m	
X-ray diffraction	Bragg pattern of a single crystal. Crystal structure (calcite) could be solved.	
End faces	calcite (10–14) rhombohedra	

[a] It is currently impossible to completely remove the surface organics from the tiny individuals for analysis.

TEM Investigations on FIB Cuts of Artificial Otoconia-Shaped Individuals and Human Otoconia

An initial investigation of the inner architecture of the artificial otoconia-shaped individuals was based on SEM images, which indicated the presence of two different structures: a more dense, homogeneous structure and a more porous one.[9] This was followed by a more detailed TEM investigation by means of thin focussed ion beam (FIB) cuts through the branch and belly regions of an artificial specimen in an early growth state (Figure 5, a and b). The belly region is only poorly crystalline and comprises nanodomains in a mosaic arrangement as well as pores (Figure 5, c). The high-resolution TEM image of the branch area shows a perfectly periodic calcite pattern (Figure 5, d). This reflects the dense composite structure, which is additionally

streaked with parallel traces (Figure 6, a) of about 25 nm periodicity. This is confirmed by the corresponding fast Fourier transform (FFT) processed image (Figure 6, b), which gives rise to superstructure lattice diffraction spots (marked by white arrows).

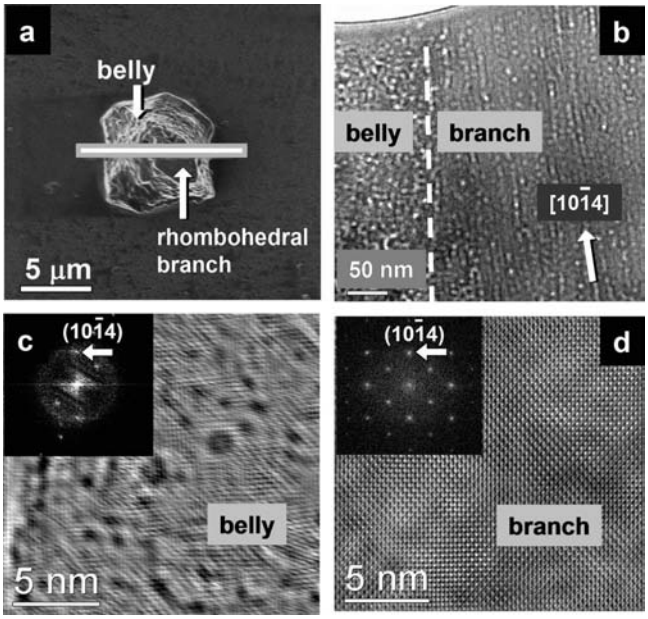

Figure 5. (a) Ion scanning image of an artificial, otoconia-shaped specimen at an early stage of morphogenesis (Figure 3, state 2). The bar indicates the area from which the TEM lamella was cut by the FIB technique. The cut leads through one branch oriented along the viewing direction. (b) Overview TEM image of the FIB thin cut showing the structure of the composite, which comprises two different areas (belly and branch). (c) The belly region (filtered high-resolution TEM image) is only poorly crystalline and consists of nanodomains in a mosaic arrangement as well as pores. Compared with the branch area, the FFT of the belly region (inset top left) displays only a small number of weak spots due to reduced crystallinity. (d) As evidenced by the filtered high-resolution TEM image, the branch area exhibits a perfect periodic pattern. As deduced from the FFT, the calcite composite is viewed along [42-6-1] (taken from ref[9b]).

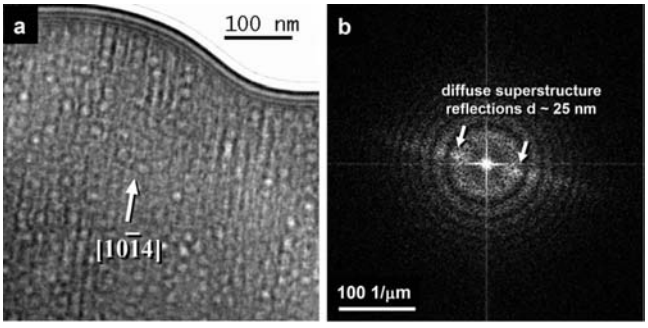

Figure 6. (a) The branch region of artificial, otoconia-shaped individuals is dominated by parallel orientation of mineralised protein fibrils running along [10-14]. (b). The FFT of (a) indicates a superstructure caused by the ordering of the mineralised fibrils and appears as diffuse diffraction spots (marked with white arrows) with a spacing of about 25 nm.

In analogy to our experience with apatite–gelatine nanocomposite structures[20–24] and in accordance with the hollow tubes visible in partially decalcified otoconia (vide infra) we interpreted these traces as signatures of (calcified) microfibrils stretching along the main branch direction [10-14]. The overall crystallographic orientation of the belly and branch areas are identical, which fully agrees with the X-ray Bragg diffraction properties of the completely developed artificial specimens (Figure 4).

Further investigations on thin cuts of embryonic states (corresponding to state 3 in Figure 2) of the artificial individuals revealed that the six branches meet close to a common point in the centre of the aggregate as shown in Figure 7. From these data, we constructed a model of the inner architecture of the otoconia-shaped individuals, which resulted in a dumbbell-shaped entity formed by the compact branch parts as displayed in Figure 8 (a). The orientation of the organic fibrils within the branch areas is indicated in Figure 8 (b) by white arrows (parallel orientation perpendicular to the rhombohedral end faces).

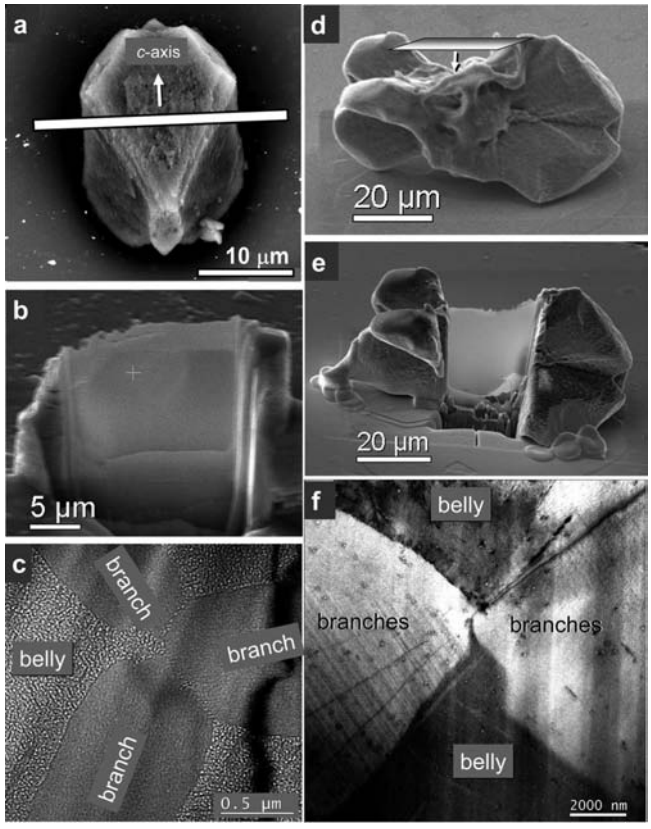

Figure 7. Cross-sectional (a–c) and longitudinal (d–f) FIB thin cuts of the embryonic states (corresponding to state 3 in Figure 2) of artificial, otoconia-shaped individuals showing the six branches meeting nearly in a common point in the centre of the aggregate (c and f).

In case of human otoconia, we found the same arrangement of branches and fibrils. Figure 9 (a) shows a longitudinal FIB cut of a human otoconial specimen with the corresponding electron diffraction pattern of the whole cut (Figure 9, b), which is again representative of a single crystal in

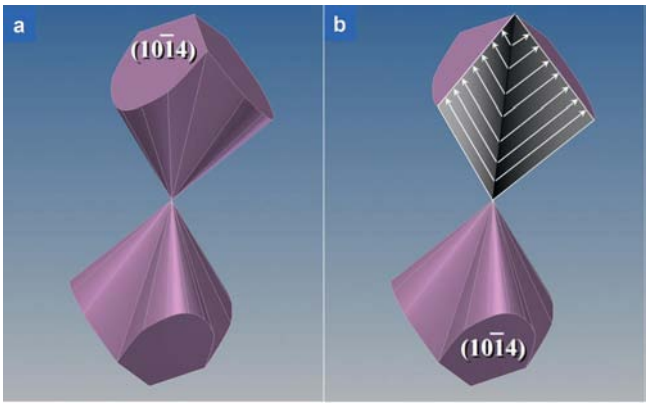

Figure 8. (a) Model of the inner architecture of artificial (otoconia-shaped) composite individuals and human otoconia that results in a dumbbell-shaped entity of the compact branch parts. (b) View inside the dumbbell: The orientation of the organic fibrils within the branch areas (perpendicular to the rhombohedral faces) is indicated by white arrows.

the sense of a mesocrystal.[25] The branches form the rhombohedral end faces with parallel orientation of the fibrils. As with the artificial individuals, we found fibril packing with about 20 nm periodicity, and a more disordered belly part (Figure 9, c). In Figure 9 (d), the interface of two branches is indicated by a dashed line. In both branches the fibrils run parallel to [10-14], normal to the facet surfaces.

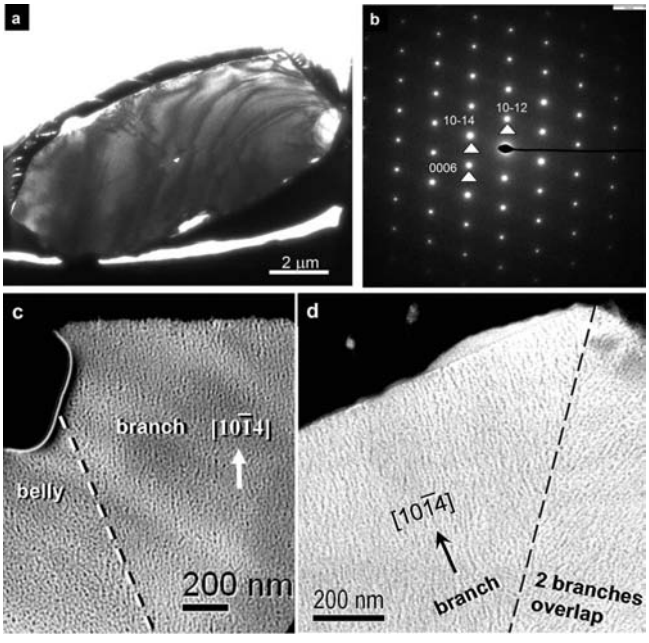

Figure 9. (a) TEM image of a longitudinal FIB cut of a human otoconial specimen. (b) Diffraction pattern of the complete cut (a), which corresponds to the [1 1 0] zone of calcite and indicates single-crystal behaviour. (c) The denser branch area (forming the rhombohedral end face) and the less ordered belly part. (d) Left: Branch area with [10-14] orientation of calcite that contains fibrils in a parallel arrangement running normal to the rhombohedral face (packing sequence of the fibrils: ca. 20 nm periodicity). Right: Overlap of two branches in the direction of view.

A cross-sectional FIB cut of human otoconia is presented in Figure 10 (b), with the cut running parallel to the largest diameter of the trumpet-shaped branches marked by the green frame in Figure 10 (a).

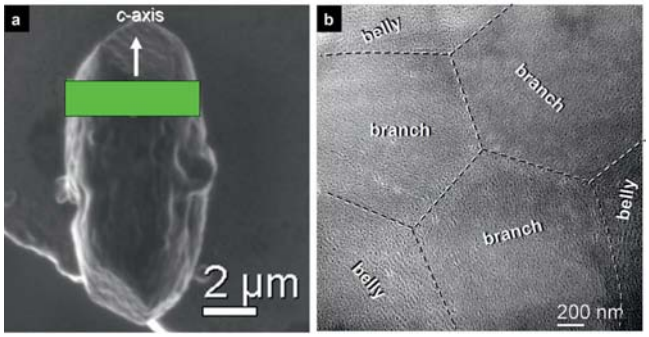

Figure 10. (a) SEM image of a human otoconial individual. The green bar indicates the cross-sectional FIB cut that runs parallel to the largest diameter of the branches. (b) TEM micrograph of the FIB cut with merging branches in the centre surrounded by the belly area.

Decalcification of Artificial (Otoconia-Shaped) Individuals and Human Otoconia

As shown in Figure 11, the artificial composite specimens can be decalcified by treatment with ethylenediaminetetraacetic acid (EDTA). The gelatineous residue keeps the shape of the former calcite–gelatine composite, which was also observed for decalcified rat otoconia.[11] The decalcification behaviour of human otoconia can be observed on age-related degenerated human otoconia, which reveals clear signs of decalcification. Such a degenerated human otoconial specimen is presented in Figure 12, with the belly area already partially dissolved and streaked with larger channels. The rhombohedral branches, however, remain more or less unaffected, which is consistent with the observations made on artificial otoconia-shaped individuals (Figure 11). Age-related degenerated human otoconia have already been the subject of an SEM investigation,[11] which revealed similar degeneration patterns to those shown in Figure 12 (a). In addition, we investigated mechanically broken specimens of age-related degenerated human oto-

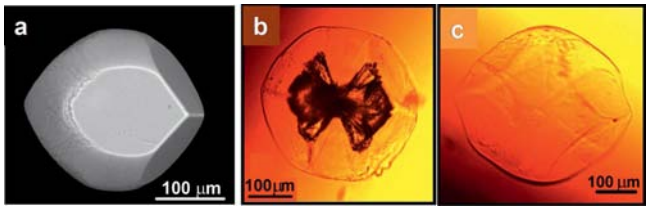

Figure 11. (a) SEM image of an artificial otoconia-shaped specimen. (b and c) Optical micrographs of successive decalcification by EDTA (c = 0.25 mol L^{-1}), which reveal that the belly parts are more easily decalcified than the branch parts. This confirms the different density of the structures. (b) After treatment with EDTA for 1 h. The belly parts have almost completely vanished whereas the dumbbell shaped trumpets are remaining. (c) After treatment with EDTA for 2 h. The inorganic component is completely removed. The decalcified gelatine, however, keeps the shape of the former composite.

conia. Figure 12 (b) shows the exposed inner structure, which contains the three branch parts as residual stumps. These results are supported by SEM investigations of the fracture area of biogenic otoconia close to the triplanar faceted ends obtained from guinea pig, which reveal the presence of three distinct regions[9,29] that are now interpreted as the branch areas.

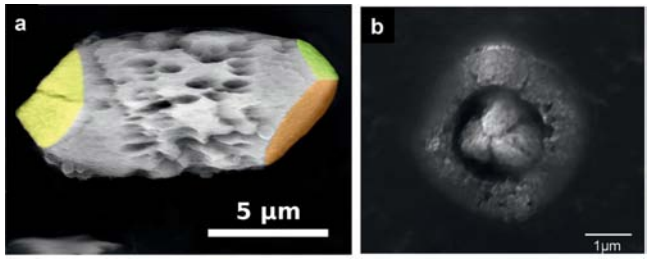

Figure 12. (a) SEM image of an age-related degenerated specimen of human otoconia with coloured rhombohedral end faces. The belly area is significantly dissolved, whereas the rhombohedral branches are nearly unaffected. (b) Mechanically broken specimen of age-related degenerated human otoconia containing the three branch parts as residual stumps.

Figure 13 shows SEM images of age-related degenerated human otoconia together with artificial composite specimens after partial decalcification. In accordance with the TEM investigations, which indicate a denser structure for the branches, the SEM image clearly reveals that these regions are less soluble compared with the porous, less ordered belly area. It becomes evident from the SEM images (Figure 13) that the interactions between the organic and inorganic components of the artificial and biogenic composites take place at a high level of structural order. During

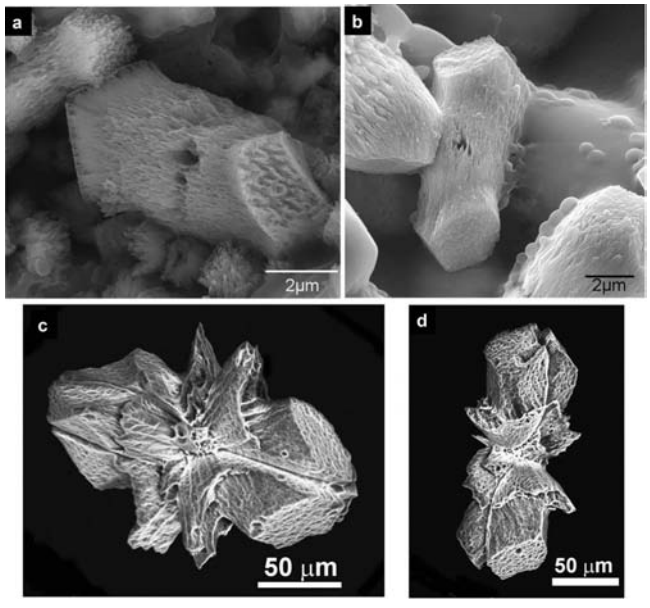

Figure 13. Comparison of SEM images of age-related degenerated human otoconia (a and b) with artificial otoconia-shaped specimens after partial decalcification by EDTA (c and d). In accordance with the TEM investigations, which indicate a denser structure for the branches, the SEM images clearly reveal that these regions are less soluble compared to the porous, less ordered belly area.

treatment of artificial individuals with EDTA, the dissolution of calcite preferably starts at the defect positions, which are generated by the heterogeneous interaction between the calcite matrix and the gelatine microfibrils. Therefore, the region of calcite around the microfibrils is dissolved faster. After treatment with warm water the demineralised gelatine microfibrils are removed. The orientation and position of the etched pits reproduces the original orientation and position of the organic microfibrils within the aggregate. Therefore, the hollow tubes that appear on the rhombohedral faces of the artificial individuals and the human otoconia represent the positions of the former organic fibrils that extend from the inner part of the composite structure in direction of the faces at both ends of the specimens (see Figures 5, 6, 8 and 9).

Organic Components Involved in the Formation of Otoconia and the Calcite–Gelatine Composite Individuals

Otoconia of mammals contain glycoproteins and glycosaminoglycans (in addition to other organic components),[30] which form fibrils inside the composite structure.[8,10,13] It is generally accepted that the different $CaCO_3$ polymorphs in otoconia and otholiths are associated with a unique protein: otoconin.[31] In calcite otoconia of mammals and birds, the major protein is a highly glycosylated glycoprotein named otoconin 90 (more than 90% of the soluble organic matrix).[32,33] The principal insoluble scaffold protein otolin contributes to the extracellular matrix of the inner ear and is responsible for the growth and anchoring of otoconia.[30,34,35] This protein has also been identified and partially characterised in otoliths of fish (teleosts) and is called otolin-1.[34] However, otolin and/or otolin-like proteins have also been identified in mammalian otoconial complexes and inner ear tissues.[30,35] Otolin is a collagenous protein belonging to the type X collagen family. The artificial otoconia-shaped individuals presented here are grown in a pure gelatine gel (denatured collagen), which is generally assumed to consist of the fiber protein without saccharide interconnections. With this knowledge, we simply mixed agarose (which is also known to be incorporated into calcite single crystals during growth)[36] with gelatine (wt.-ratio 7:3) and used the respective gel mixture as the diffusion matrix.[9] As can be seen from Figure 14, the more bulbous

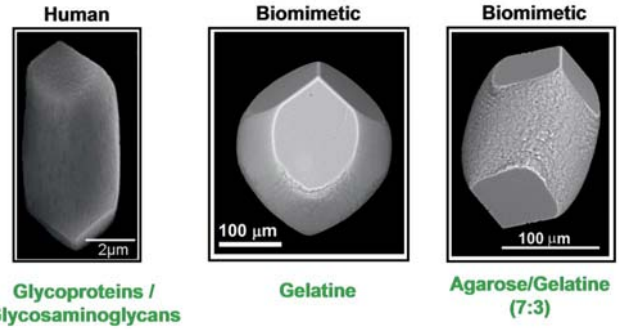

Figure 14. Morphology (SEM images) of otoconia-shaped individuals: Biogenic/human (left), artificial/gelatine (middle), artificial/agarose–gelatine (right).

belly region of the artificial composite individuals can be flattened and elongated, which reveals a closer relationship to the shape of human otoconia.

The reason for this significant change in morphology from adding agarose to the gelatine-gel matrix is not known and will be investigated in the future. Atomistic simulations (in aqueous systems) have successfully been used for the investigation of nucleation scenarios of motifs of the apatite crystal structure at/in triple-helical collagen molecules (formation of bone and teeth).[37] With respect to the present problem concerning nucleation and growth of otoconia, we started to investigate the nucleation of calcium carbonate at biomacromolecules. As a preliminary result, we found that calcium carbonate is best nucleated at otolin that contains disaccharide side chains.[38] With this in mind and the fact that commercial gelatine still contains 0.5-1.0 wt.-% covalently bound saccharides,[39] the situation becomes a bit more consistent. However, a lot of essential questions remain unanswered, which is also true for a more general characterisation of the outer shape of otoconia as this is still at a descriptive level and no definite rules that concern aspect ratios and other quantifying criteria are known to date.

Conclusions

The chemical and structural characteristics of calcite–gelatine composites grown by double diffusion in gelatine-gel matrices are closely related to biogenic (human) otoconia. This conclusion is true not only for their inner composite architecture but also for their outer shape, which makes this study the first example of a successful imitation of a biomineral (inner architecture and outer shape). The artificial system is a suitable model system with which to investigate a number of essential problems with respect to nucleation, morphogenesis and the function of biogenic otoconia. Concerning the function of otoconia, their inner density distribution (dumbbell-shaped, more compact branch areas and more porous, less ordered belly areas) seems to be of essential importance and may cause optimum movement response on acceleration scenarios. With the inner branch/belly architecture it is also possible to reinterpret some reports on the presence of a core/shell structure in biogenic otoconia.[8,10,15] These images represent longitudinal scratches through the belly region, which are significantly shifted from the centre of the individuals, and touch parts of the branches and their ends.

Experimental Section

Materials: Samples of human otoconia (used for our investigations) were isolated by Dr. Yu. Yarin. The specimens were processed according to the standard techniques described in several publications.[8,10,14,26]

Synthesis: The growth of calcite–gelatine composites by double diffusion into a gelatine-gel matrix is described in ref.[9]

X-ray Crystallography: Investigations of artificial (otoconia-shaped) individuals are described in ref.[9] A complete human otoconial specimen was investigated with a Rigaku R-AXIS SPIDER with Ag-K_α radiation (0.56087 Å). Face indexing of an otoconia-shaped artificial specimen in its final state of development was performed by using the X-shape procedure (Stoe & Cie GmbH).

The crystal structures of completely developed individuals (artificial//biogenic) were investigated (radiation: Mo-K_α//Ag-K_α; reflections: collected 1159//535; independent 140//119; R_{int} 0.016//0.078; $N(hkl)$ with $I > 2\sigma$ (I) (used for refinement) 140//106) and refined in space group $R\bar{3}c$: a_H = 4.9880(4)//4.9836(7) Å, c_H = 17.096(2)// 17.071(4) Å, z_H = 6. Ca: 0, 0, 0//0, 0, 0 with U_{eq}(Å^2): 0.0152(2)// 0.0275(10); C: 0, 0, 0.25//0, 0, 0.25 with U_{eq}(Å^2): 0.0123(5)// 0.021(2); O: 0.2571(3), 0, 0.25// 0.2567(12), 0, 0.25 with U_{eq}(Å^2): 0.0244(3)//0.0344(16); $R(F_o)$ = 0.025//0.068.

CCDC-423567 (for the artificial sample) and -423568 (for the biogenic sample) contain the supplementary crystallographic data for this paper. These data can be obtained free of charge from The Cambridge Crystallographic Data Centre via www.ccdc.cam.ac.uk/data_request/cif.

Decalcification: The calcite–gelatine composites were decalcified by treatment with EDTA (c = 0.25 mol L^{-1}) for varying periods of time. Optical microscopy images of partially and totally demineralised individuals were taken with the "Axioplan 2 imaging" microscope (Carl-Zeiss, Oberkochen, Germany). For SEM investigations of partially decalcified particles, the samples were washed twice in distilled water at 40 °C (in order to remove the demineralised gelatine from the surface of the aggregates), centrifuged and dried at 40 °C.

SEM: The morphology and inner structure of the aggregates were studied by SEM and TEM. SEM investigations were performed with an ESEM FEI Quanta 200 FEGi system operated in low (60 Pa) and high vacuum mode (2×10^{-4} Pa) at acceleration voltages between 15–25 kV (FEI, Eindhoven, NL). For investigation under high vacuum, the samples were coated with a thin gold layer (for 30 seconds) in order to obtain a conductive surface.

FIB Thin Cut Preparation: For TEM investigations FIB thin cuts of the aggregates were prepared with a FEI Quanta 200 3D dual beam device (FEI, Eindhoven, NL). For this purpose, selected particles were deposited from an ethanol suspension onto a copper half ring and the selected region was covered with a protective layer of platinum (thickness 1–2 μm, acceleration voltage 30 kV, current 0.3 nA). After this preparation, the particles were thinned down to electron transparency (thickness of 100–200 nm) by the FIB system at 30 kV acceleration voltage, currents of 3–0.05 nA for the Ga^+ beam.

TEM: The TEM experiments on the artificial samples were carried out at the Special Laboratory Triebenberg for Electron Holography and High-Resolution Microscopy at the TU Dresden. A field emission microscope CM 200 FEG/ST-Lorentz (FEI, Eindhoven, NL) equipped with a Gatan 1 × 1 k slow scan CCD camera was used. The analyses of the TEM images were realised the Digital Micrograph software (Gatan, USA). TEM measurements of the human otoconia were performed with a FEI Tecnai 10 electron microscope (FEI, Eindhoven, NL) with a LaB_6 source at 100 kV acceleration voltage. Images were recorded with a Tietz slow scan CCD F224HD TVIPS camera (2k × 2k pixels, pixel size 24 μm, digitisation 16 bit) with an active area of 49 × 49 mm. (Tietz Video and Image Processing Systems GmbH, Gauting, Germany).

Acknowledgments

We would like to acknowledge fruitful cooperation and discussions with Prof. Dr. Hans-Jürgen Hardtke and Prof. Dr. Rolf Schmidt (Institut für Festkörpermechanik der TU Dresden). We would also like to thank Prof. Dr. Hannes Lichte for the opportunity to perform TEM measurements at the Triebenberg Laboratory (TU Dresden). Sincere thanks are given to Dr. Steffen Wirth (MPI CPfS) for continuous help.

[1] W. Kahle, M. Frotscher, *Color Atlas and Textbook of Human Anatomy*, vol. 3, *Nervous System and Sensory Organs*, 5th ed., Thieme Medical Publishers, Stuttgart, Germany, **2003**.
[2] *Biomineralisation: Cell Biology and Mineral Deposition* (Eds.: K. Simkiss, K. M. Wilbur), Academic Press, San Diego, **1989**.
[3] *Biomineralisation: Progress in Biology, Molecular Biology and Application* (Ed.: E. Bäuerlein), Wiley-VCH, Weinheim, **2004**.
[4] *Handbook of Biomineralization: Biological Aspects and Structure Formation* (Ed.: E. Bäuerlein), Wiley-VCH, Weinheim, Germany, **2007**.
[5] L. Addadi, S. Weiner, *Angew. Chem.* **1992**, *104*, 159–176; *Angew. Chem. Int. Ed. Engl.* **1992**, *31*, 153–169.
[6] *Biomineralisation and Biological Metal Accumulation* (Eds.: P. Westbroek, E. W. de Jong), D. Reidel Publ. Comp., Dordrecht, NL, **1983**.
[7] M. D. Ross, K. G. Pote, *Philos. Trans. R. Soc. London Ser. B* **1984**, *304*, 445.
[8] U. Lins, M. Farina, M. Kurc, G. Riordan, R. Thalmann, I. Thalmann, B. Kachar, *J. Struct. Biol.* **2000**, *131*, 67–78.
[9] a) Y.-X. Huang, R. Cardoso Gil, Yu. Prots, P. Simon, W. Carrillo-Cabrera, J. Buder, *Abstracts, ECSSC XI.* **2007**, *W11*, 163; b) Y.-X. Huang, J. Buder, R. Cardoso-Gil, Yu. Prots, W. Carrillo-Cabrera, P. Simon, R. Kniep, *Angew. Chem.* **2008**, *120*, 8404–8408; *Angew. Chem. Int. Ed.* **2008**, *47*, 8280–8284; c) R. Kniep, *BioSpektrum* **2009**, *15*, 498–500; d) Y.-X. Huang, J. Buder, H. Borrmann, R. Cardoso-Gil, W. Carrillo-Cabrera, Yu. Prots, P. Simon, R. Kniep, *Scientific Report 2006-2008 MPI CPfS*, Dresden, Germany, **2009**, 218–225; e) R. Kniep, *Nachr. Chem.* **2010**, *58*, 419–423.
[10] S. Mann, S. B. Parker, M. D. Ross, A. J. Skarnulis, R. J. P. Williams, *Proc. R. Soc. London Ser. B Proc. R. Soc. London B* **1983**, *218*, 415–424.
[11] M. D. Ross, D. Peacor, L.-G. Johnsson, L. F. Allard, *Ann. Otol. Rhinol. Laryngol.* **1976**, *85*, 310–326.
[12] H. Li, L. A. Estroff, *J. Am. Chem. Soc.* **2007**, *129*, 5480–5483.
[13] C. D. Fermin, *Microsc. Res. Tech.* **1993**, *25*, 297–303.
[14] M. D. Ross, K. G. Pote, F. Perini, in: *Auditory Biochemistry* (Ed.: D. G. Drescher), C. C. Thomas, Springfield, IL, USA, **1984**, pp. 351–365.
[15] K. G. Pote, M. D. Ross, *J. Ultrastruct. Mol. Struct. Res.* **1986**, *95*, 61–70.
[16] C. G. Wright, D. G. Hubbard, *Acta Oto-Laryngol.* **1978**, *86*, 185–194.
[17] L. A. Everett, I. A. Belyantseva, K. Noben-Trauth, R. Cantos, A. Chen, S. I. Thakkar, S. L. Hoogstraten-Miller, B. Kachar, D. K. Wu, E. D. Green, *Hum. Mol. Gen.* **2001**, *10*,153–161.
[18] D. Carlstrom, H. Engstrom, *Acta Oto-Laryngol.* **1955**, *45*, 14–18.
[19] D. Carlstrom, *Biol. Bull.* **1963**, *125*, 441–463.
[20] P. Simon, D. Zahn, H. Lichte, R. Kniep, *Angew. Chem.* **2006**, *118*, 1945–1949; *Angew. Chem. Int. Ed.* **2006**, *45*, 1911–1915.
[21] P. Simon, W. Carrillo-Cabrera, P. Formanek, C. Göbel, D. Geiger, R. Ramlau, H. Tlatlik, J. Buder, R. Kniep, *J. Mater. Chem.* **2004**, *14*, 2218–2224.
[22] P. Simon, U. Schwarz, R. Kniep, *J. Mater. Chem.* **2005**, *15*, 4992–4996.
[23] H. Tlatlik, P. Simon, A. Kawska, D. Zahn, R. Kniep, *Angew. Chem.* 2006, ***118***, 1939–1944; *Angew. Chem. Int. Ed.* **2006**, *45*, 1905–1910.
[24] R. Kniep, P. Simon, *Angew. Chem.* **2008**, *120*, 1427–1431; *Angew. Chem. Int. Ed.* **2008**, *47*, 1405–1409.
[25] a) H. Cölfen, M. Antonietti, *Angew. Chem.* **2005**, *117*, 5714–5730; *Angew. Chem. Int. Ed.* **2005**, *44*, 5576–5591; b) H. Cölfen, M. Antonietti, *Mesocrystals and Nonclassical Crystallisation*, Wiley, Chichester, UK, **2008**.
[26] K. G. Pote, C. H. Weber, R. H. Kretsinger, *Hear. Res.* **1993**, *66*, 225–232.
[27] E. V. Rosseeva, J. Buder, P. Simon, U. Schwarz, O. V. Frank-Kamenetskaya, R. Kniep, *Chem. Mater.* **2008**, *20*, 6003–6013.
[28] J. D. Dickman, D. Huss, M. J. Lowe, *Hearing Research* **2004**, *188*, 89–103.
[29] C. P. Hommerich, R. Kniep, *Jahresversammlung Deutsche Gesellschaft für Hals-Nasen-Ohren-Heilkunde*, Würzburg, Germany, **1986**, 57.
[30] Y. W. Lundberg, X. Zhao, E. N. Yamoah, *Brain Res.* **2006**, *1091*,47–57.
[31] K. G. Pote, M. D. Ross, *Comput. Biochem. Physiol. B* **1991**, *98*, 287–295.
[32] Y. Wang, P. E. Kowalski, I. Thalmann, D. M. Ornitz, D. L. Mager, R. Thalmann, *Proc. Natl. Acad. Sci. USA* **1998**, *95*, 15345–15350.
[33] W. Lu, D. Zhou, J. J. Freeman, I. Thalmann, D. M. Ornitz, R. Thalmann, *Hearing Research* **2010**, *268*, 172–183.
[34] a) E. Murayama, Y. Takagi, H. Nagasawa, *Cell Biol.* **2004**, *121*, 155–166; b) E. Murayama, P. Herbomel, A. Kawakami, H. Takeda, H. Nagasawa, *Mechanisms Development* **2005**, *122*, 791–803.
[35] M. R. Deans, J. M. Peterson, G. W. Wong, *PLoS One* **2010**, *5*, 12765.
[36] H. Li, H. L. Xin, D. A. Müller, L. E. Estroff, *Science* **2009**, *326*, 1244–1247.
[37] A. Kawska, O. Hochrein, J. Brickman, R. Kniep, D. Zahn, *Angew. Chem.* **2008**, *120*, 5060–5063; *Angew. Chem. Int. Ed.* **2008**, *47*, 4982–4985.
[38] P. Duchstein, R. Kniep, D. Zahn, manuscript to be submitted.
[39] T. Koide, K. Nagata, in: *Top. Curr. Chem.: Collagen Primer in Structure, Processing and Assembly* (Eds.: J. Brinckmann, H. Notbohm, P. K. Müller), Springer, Berlin Heidelberg, Germany, **2005**, vol. 247, pp. 85–114.

Received: July 20, 2011
Published Online: October 26, 2011

